ACS APPLIED MATERIALS & INTERFACES

Research Article

www.acsami.org

Interfacial Octahedral Rotation Mismatch Control of the Symmetry and Properties of $SrRuO_3$

Ran Gao,[†] Yongqi Dong,[‡] Han Xu,[‡] Hua Zhou,[§] Yakun Yuan,[∥] Venkatraman Gopalan,[∥] Chen Gao,[‡] Dillon D. Fong,[⊥] Zuhuang Chen,*[,†,#] Zhenlin Luo,[‡] and Lane W. Martin*[,†,#]

[†]Department of Materials Science and Engineering, University of California, Berkeley, California 94720, United States

[‡]National Synchrotron Radiation Laboratory and CAS Key Laboratory of Materials for Energy Conversion, University of Science and Technology of China, Hefei, Anhui 230026, People's Republic of China

[§]X-ray Science Division, Advanced Photon Source, Argonne National Laboratory, Argonne, Illinois 60439, United States

[∥]Department of Materials Science and Engineering, Pennsylvania State University, State College, Pennsylvania 16802, United States

[⊥]Materials Science Division, Argonne National Laboratory, Argonne, Illinois 60439, United States

[#]Materials Science Division, Lawrence Berkeley National Laboratory, Berkeley, California 94720, United States

Supporting Information

ABSTRACT: Epitaxial strain can be used to tune the properties of complex oxides with perovskite structure. Beyond just lattice mismatch, the use of octahedral rotation mismatch at heterointerfaces could also provide an effective route to manipulate material properties. Here, we examine the evolution of the structural motif (i.e., lattice parameters, symmetry, and octahedral rotations) of $SrRuO_3$ films grown on substrates engineered to have the same lattice parameters, but different octahedral rotations. $SrRuO_3$ films grown on $SrTiO_3$ (001) (no octahedral rotations) and $GdScO_3$-buffered $SrTiO_3$ (001) (with octahedral rotations) substrates are found to exhibit monoclinic and tetragonal symmetry, respectively. Electrical transport and magnetic measurements reveal that the tetragonal films exhibit higher resistivity, lower magnetic Curie temperatures, and more isotropic magnetism as compared to those with monoclinic structure. Synchrotron-based quantification of the octahedral rotation network reveals that the tilting pattern in both film variants is the same (albeit with slightly different magnitudes of in-plane rotation angles). The abnormal rotation pattern observed in tetragonal $SrRuO_3$ indicates a possible decoupling between the internal octahedral rotation and lattice symmetry, which could provide new opportunities to engineer thin-film structure and properties.

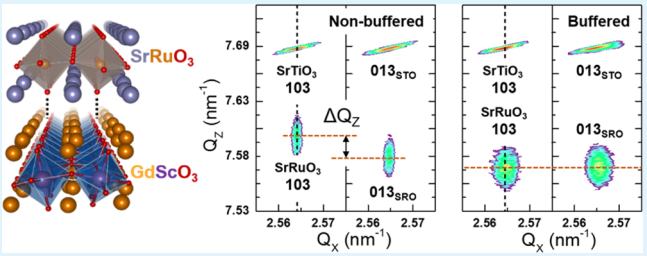

KEYWORDS: *$SrRuO_3$, epitaxial strain, octahedral rotation, interfacial engineering, crystal symmetry*

INTRODUCTION

ABO_3 perovskite oxides exhibit a diverse range of functional properties which can be readily manipulated thus making such materials candidates for a wide range of applications (e.g., logic,[1,2] memories,[3] sensing,[4] and photovoltaics[5]). The tunable nature of such materials arises from the strong coupling between charge, orbital, spin, and lattice degrees of freedom present in these systems. In films of such materials the use of epitaxial strain enables direct manipulation of the lattice degree of freedom and subsequent control of charge, orbital, and spin physics.[6−8] Taking the canonical itinerant ferromagnetic $SrRuO_3$ as an example,[9] ferromagnetism can be quenched under application of epitaxial strain due to a suppression of the octahedral rotations that fundamentally changes the density of states of spin-up and -down electrons at the Fermi level.[10−12] In turn, $SrRuO_3$, which exhibits orthorhombic symmetry in the bulk, can be driven, under relatively large tensile or compressive strains, to exhibit tetragonal symmetry.[13,14]

In addition to epitaxial strain induced by lattice mismatch, an alternative interfacial coupling effect can also take place when there exists an octahedral rotation mismatch between substrate and film.[15−17] Due to differences in the ionic radii of the *A*- and *B*-cations and oxygen and the semi-rigidity of the oxygen octahedra cage, some perovskites exhibit octahedral rotations which can be described as a combination of rotations along three orthogonal axes ([100], [010], and [001] in the pseudocubic unit cell) with angles α, β, and γ (Figure 1a).[18−20] Using Glazer notation, the relative magnitudes of the rotation along the three axes are denoted as *a*, *b*, and *c*, superscripted by 0, +, or − to indicate no rotation, in-phase rotation, or out-of-phase rotation, respectively.[18] When a material with robust octahedral rotations is intimately coupled

Received: March 8, 2016
Accepted: May 24, 2016
Published: May 24, 2016

DOI: 10.1021/acsami.6b02864
ACS Appl. Mater. Interfaces 2016, 8, 14871−14878

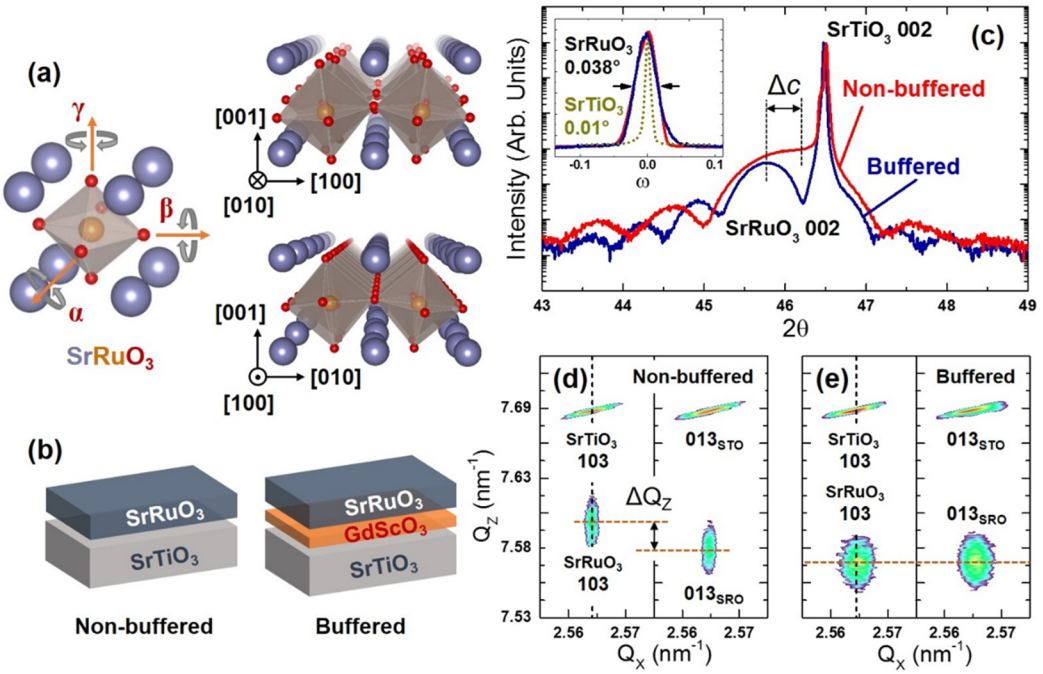

Figure 1. (a) Pseudocubic unit cell of $SrRuO_3$ including two perspective views along [010] and [100], corresponding to out-of-phase (−) and in-phase (+) octahedral rotation axis, respectively. (b) Sample design for interfacial octahedral rotation mismatch studies. (c) X-ray θ−2θ scans about the 002 pseudocubic diffraction conditions for 10 nm thick nonbuffered and buffered $SrRuO_3$ films. Inset shows the rocking curves of the films and substrate with the corresponding full width at half-maximum values. Reciprocal space mapping studies about the 103 and 013 pseudocubic diffraction conditions of (d) nonbuffered and (e) buffered $SrRuO_3$.

with another material that exhibits no or smaller octahedral rotations, the mismatch of atomic displacement at the heterointerface is generally accommodated by either deforming or rotating the oxygen octahedra in the film.[15,17]

Despite the potential for these different modes of heterointerfacial coupling, the pervasive approach in the study of epitaxial strain has been to consider only the role of lattice mismatch-induced strain while neglecting or downplaying the role of octahedral rotation mismatch (which is hard to quantify and investigate). In fact, only in recent years have researchers started to probe the effects of such octahedral rotation mismatch in systems such as $BiFeO_3/La_{0.7}Sr_{0.3}MnO_3$,[21] $LaAlO_3/SrTiO_3$,[22] and $(LaNiO_3)_n/(SrMnO_3)_m$ superlattices[23] using state-of-the-art transmission electron microscopy and synchrotron-based X-ray diffraction. Despite these studies, a complete physical picture of such interactions and understanding of the length scales over which such effects can extend are still being developed. Nonetheless, it is becoming clear that in order to exert deterministic control over such heterostructures, knowledge of both the lattice and octahedral rotation mismatch effects are needed. This is particularly important when one considers that at room temperature most commercially available substrates used for perovskite growth possess orthorhombic $(a^-a^-c^+)$ or rhombohedral $(a^-a^-a^-)$ symmetry with robust octahedral rotations.[24−27] Thus, the effects of lattice mismatch could be convoluted by additional contributions from the interfacial octahedral rotation mismatch. Finally, with the increasing study of ultrathin heterostructures and superlattices, where interfacial octahedral rotation coupling could potentially play a more dominant role in controlling film properties, such understanding is essential.

In this spirit, we use $SrRuO_3$ as a model system to examine how interfacial octahedral rotation mismatch contributes to the micro-/macroscopic structural and physical properties. In order to examine the effects of octahedral rotation mismatch alone, we explore 10 nm $SrRuO_3$ films grown directly on bare, cubic $SrTiO_3$ (001) and on 4 nm, orthorhombic $GdScO_3$-buffered $SrTiO_3$ (001) substrates which leverages a strategy to control the lattice parameters and octahedral rotations simultaneously.[28] By changing the octahedral rotation mismatch at the $SrRuO_3/SrTiO_3$ interface with the addition of a few nanometers of $GdScO_3$, one can dramatically change the crystal symmetry and properties of the $SrRuO_3$. In $SrRuO_3/SrTiO_3$ (001) heterostructures, $SrRuO_3$ exhibits monoclinic lattice symmetry with strong magnetic anisotropy, and a Curie temperature (T_C) of 148 K. In $SrRuO_3/GdScO_3/SrTiO_3$ (001) heterostructures, the $SrRuO_3$ lattice symmetry is tetragonal and the heterostructures exhibit a higher overall film resistivity, nearly isotropic in-plane magnetic behavior, and a lower T_C = 143 K. Subsequent synchrotron-based diffraction and half-order superstructure Bragg peak analyses reveal that although the lattice symmetry is changed, both the monoclinic and tetragonal variants of $SrRuO_3$ have the same internal octahedral rotation pattern $(a^+b^-c^-)$ albeit with a slightly smaller in-plane rotation angle in the tetragonal variant. Such an orthorhombic octahedral rotation pattern in a tetragonal lattice indicates a possible decoupling between lattice symmetry and internal octahedral rotation symmetry and highlights the significance of interfacial octahedral rotation mismatch as a potential pathway to engineer perovskite materials.

EXPERIMENTAL SECTION

Thin-Film Growth. All films were grown via pulsed-laser deposition. Prior to growth, the $SrTiO_3$ substrates were treated by chemical etching and annealing following standard procedures.[29] The $GdScO_3$-buffer layer was grown at 680 °C in 7.5 mTorr of oxygen with a laser fluence of 1.5 J/cm^2 at a repetition rate of 5 Hz (a total of 140

DOI: 10.1021/acsami.6b02864
ACS Appl. Mater. Interfaces 2016, 8, 14871−14878

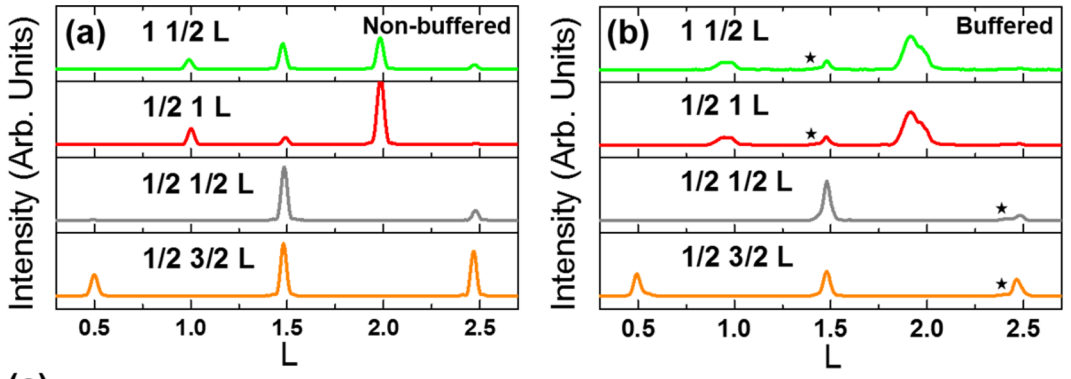

(c)

	Octahedral Rotation Angle (°)			Variant Ratio (%)			
	α	β	γ	X	Y	X'	Y'
Non-Buffered	6.2 ± 1.3	6.8 ± 1.4	7.4 ± 1.5	33.2	12.5	35.7	18.6
$GdScO_3$-Buffered	5.7 ± 1.6	5.9 ± 1.9	7.2 ± 1.4	20.8	23.2	30.6	25.4
Bulk	6.19	5.97	5.97	-	-	-	-

Figure 2. Four representative half-order Bragg peak diffraction patterns for 10 nm thick (a) nonbuffered and (b) buffered $SrRuO_3$. Peaks from the $GdScO_3$-buffer layer are marked with an asterisk (*). (c) Experimentally measured and extracted octahedral rotation angles and domain variant fractions as obtained from the half-order Bragg peaks analysis.

pulses yielded 4 nm thick films). The $SrRuO_3$ films were grown at 680 °C in 100 mTorr of oxygen with a laser fluence of 1.5 J/cm^2 and a repetition rate of 5 Hz (a total of 750 pulses yielded 10 nm thick films). Following growth, the heterostructures were cooled at 5 °C/min. in a static oxygen pressure of 760 Torr. Furthermore, to rule out the effects of varying vicinality in the $SrTiO_3$ substrates,[30] $SrRuO_3$ films with or without the $GdScO_3$-buffer layer were grown on multiple pieces of the same substrate wafer.

X-ray Diffraction Studies. Laboratory-based X-ray diffraction was completed on an X'Pert MRD Pro equipped with a PIXcel detector (PANalytical). Synchrotron X-ray scans were conducted at the Advanced Photon Source, Argonne National Laboratory on beamline 12-ID-D using the Pilatus 100 K detector, and at the Shanghai Synchrotron Radiation Facility on beamline 14B.

Electronic Transport and Magnetic Measurement. Electrical transport measurements were completed in a physical properties measurement system (PPMS; Quantum Design, Inc.). During data acquisition, samples were cooled from 300 to 25 K at 5 K/min. For magnetic measurements a magnetic property measurement system (MPMS; Quantum Design) was used. The magnetization−magnetic field hysteresis loops and magnetization−temperature profiles were obtained along two orthogonal in-plane directions (i.e., [100] and [010]) and the out-of-plane direction (i.e., [001]). In the magnetization−magnetic field measurements, samples were cooled from room temperature to 10 K in a 1 T field and held at 10 K for data acquisition. In the magnetization−temperature measurements, samples were first cooled from room temperature to 10 K in a 1 T field and then warmed at 5 K/min. to room temperature during data acquisition.

RESULTS AND DISCUSSION

We focused on 10 nm thick films of $SrRuO_3$ (bulk $SrRuO_3$ is orthorhombic with a_o = 5.567 Å, b_o = 5.530 Å, and c_o = 7.845 Å)[31] grown on $SrTiO_3$ (001) substrates (cubic, a = 3.905 Å)[25] [henceforth referred to as *nonbuffered SrRuO$_3$*] and 4 nm $GdScO_3$-buffered (bulk $GdScO_3$ is orthorhombic with a_o = 5.745 Å, b_o = 5.481 Å, and c_o = 7.929 Å)[27] $SrTiO_3$ (001) substrates) [henceforth referred to as *buffered SrRuO$_3$*]. We will use cubic or pseudocubic indices throughout unless otherwise specified (the subscript "O" will denote orthorhombic indices). A schematic view of the heterostructures is provided (Figure 1b). The design algorithm is based on the fact that there is expected to be much faster relaxation of octahedral rotation distortion at the heterointerface than lattice mismatch strain,[16,32] and thus the presence of the $GdScO_3$-buffer layer allows for one to produce the same lattice constants (as determined by the underlying substrate), but different octahedral rotation patterns and magnitudes.

X-ray diffraction studies reveal that all $SrRuO_3$ films are fully epitaxial and single phase (Supporting Information, Figure S1). Focusing about the 002 diffraction peak of the $SrRuO_3$ (Figure 1c), the buffered $SrRuO_3$ exhibits an out-of-plane lattice parameter expansion (~0.7%) as compared with nonbuffered $SrRuO_3$. Rocking curve studies reveal that all $SrRuO_3$ films are uniformly highly crystalline and that the addition of the buffer layer does not diminish the crystalline quality (inset, Figure 1c). Such a lattice expansion suggests a possible structural change of the buffered $SrRuO_3$. To further understand this structural change, reciprocal space mapping (RSM) studies were completed.

RSM studies about the 103- and 013-diffraction peaks of the $SrRuO_3$ and $SrTiO_3$ (a full set of 103-type peak scans are provided, Supporting Information, Figure S2) reveal that all diffraction peaks possess the same Q_X values confirming that the films are coherently strained (Figure 1d,e). Inspection of the peak positions in the Q_Z direction reveals that the $SrRuO_3$ 103-diffraction peak has a higher Q_Z value than the 013-diffraction peak for nonbuffered $SrRuO_3$ (Figure 1d), indicative of a monoclinic version of $SrRuO_3$ with β = 89.5°. Additional high-resolution, synchrotron-based RSMs (Supporting Information, Figure S3a) further confirm the monoclinic structure. Inspection of the peak positions in the Q_Z direction for the buffered $SrRuO_3$ (Figure 1e), however, reveals that the 103- and 013-diffraction peaks possess the same Q_Z values, indicating a tetragonal version of $SrRuO_3$, which is also supported by synchrotron-based X-ray studies (Supporting Information, Figure S3b). The observed structural change

DOI: 10.1021/acsami.6b02864
ACS Appl. Mater. Interfaces 2016, 8, 14871−14878

suggests that coupling effects between different octahedral rotation patterns at the heterointerface could be crucial in determining the film crystal symmetry. Such results call for a more comprehensive and detailed structural analysis.

Synchrotron-based half-order Bragg peak analysis has been used to extract octahedral rotation information in perovskite systems.[33,34] Based on this analysis, simple rules can be applied to understand the nature of the system: (1) in-phase octahedral rotations (+) will give rise to "even−odd−odd" half-order reflections, while out-of-phase octahedral rotations (−) will produce "odd−odd−odd" reflections; (2) in-phase rotations giving rise to even−odd−odd" reflections with $k \neq l$ are an indication of an a^+-type rotation, and those with $h \neq l$ and $h \neq k$ are indicative of b^+- and c^+-type rotations, respectively; and (3) out-of-phase rotations giving rise to odd−odd−odd reflections with $k \neq l$ are the result of a^--type rotations and those with $h \neq l$ and $h \neq k$ are the result of b^-- and c^--type rotations, respectively. Additionally, by comparing the measured and simulated intensities of certain half-order Bragg peaks, one is able to quantitatively determine the rotation angles in the pattern. Note that due to the biaxial strain exerted on the $SrRuO_3$ by the $SrTiO_3$, the octahedra in $SrRuO_3$ will have an elongation along the c axis.[7] Such effects are considered in our calculation by using appropriate lattice constants for the pseudocubic $SrRuO_3$ unit cells. Furthermore, due to the orthorhombic nature of the $SrRuO_3$ unit cell, it is possible to have four different structural domains if the material is grown on a (001)-oriented cubic substrate,[30] which we will denote as structural domains D_X, D_Y, $D_{X'}$, and $D_{Y'}$, respectively (Supporting Information, Figure S4). When we complete the fittings of the intensities of the half-order Bragg peaks, we make no *a priori* assumption about the makeup of the film as it pertains to these structural domains; thus, we can also extract the volumetric ratio of the different structural domains from these analyses.

Although over 100 *hkl* scans were performed to get accurate rotation angles and domain structures, we show (for brevity) four representative scans for each heterostructure type which are sufficient to determine the octahedral rotation patterns in the $SrRuO_3$ films. We first analyze the octahedral rotation patterns of the monoclinic, nonbuffered $SrRuO_3$ (Figure 2a). Based on the rules discussed earlier, the appearance of 1 1/2 3/2- and 1/2 1 3/2-diffraction peaks from the $SrRuO_3$ indicates that the in-phase (+) rotation is along the [100] or [010] of the $SrTiO_3$ substrate while the peak intensity difference suggests that one structural domain is dominant. In addition, we also observe 1/2 1/2 3/2-, 1/2 3/2 3/2-, and 1/2 3/2 1/2-diffraction peaks, which reveal that there are two out-of-phase rotation (−) axes that lie either in-plane or out-of-plane, but perpendicular to, the (+) axis. Therefore, we can determine that the octahedra cage in the monoclinic variant of $SrRuO_3$ is rotated along all three orthogonal directions and that the (+) axis of the rotated octahedra is aligned along either the [100] or [010] of the $SrTiO_3$ substrate resulting in two structural domains (D_X and D_Y), albeit with one of those domains dominating. Such a preference for forming one type of domain is expected due to the miscut of the $SrTiO_3$ substrate which will tend to drive the orthorhombic c axis of the $SrRuO_3$ to be aligned with the step edges of the substrates.[30]

Similar analysis can be applied to the tetragonal, buffered $SrRuO_3$. First, the appearance of half-order Bragg peaks from the $GdScO_3$-buffer layer next to those from the $SrRuO_3$ (marked with asterisks (*), Figure 2b) suggests that both layers possess a similar octahedral rotation pattern and domain structure. We note that there are additional half-order Bragg peaks from the $GdScO_3$ which are not marked due to their low intensity on the data scale provided here, but these peaks are present and have been analyzed. Further analysis of the $GdScO_3$-buffer layer reveals that it exhibits bulk-like monoclinic lattice symmetry as suggested by the increasing out-of-plane diffraction peak position difference as compared to the tetragonal $SrRuO_3$ as one moves to higher *hkl* indices (Supporting Information, Figure S5). In other words, the octahedral rotation pattern of the substrate is different when the 4 nm $GdScO_3$-buffer layer is included in the heterostructure. Upon turning our attention to the half-order Bragg peaks arising from $SrRuO_3$, however, the fitting suggests that the octahedral rotation pattern in this tetragonal variant of $SrRuO_3$ is the same as that in the monoclinic variant of nonbuffered $SrRuO_3$. At the same time, the structural domain pattern of the tetragonal, buffered $SrRuO_3$ is changed as indicated by nearly equivalent peak intensities for the 1 1/2 3/2- and 1/2 1 3/2-diffraction peaks, indicating that the D_X and D_Y structural domains have similar volumetric fractions. To summarize, using the buffer-layer approach, we can effectively tune the nature of the octahedral rotation pattern of the substrate to be different, while maintaining the same in-plane lattice parameters. In turn, this results in a change in the lattice symmetry of the $SrRuO_3$ and the structural domain fractions but does not change the octahedral rotation patterns. From here, we can further extract quantitative values for the nature of these octahedral rotations.

As noted previously, comparison of the calculated peak intensities of a full range of half-order *hkl* scans with the experimental data provides a route to extract the octahedral rotation angles and structural domain fractions for the system.[23,33,34] The fitted half-order *hkl* scans for nonbuffered and buffered $SrRuO_3$ are provided (Supporting Information, Figures S8 and S9, respectively), and the extracted rotation angles and structural domain fractions are provided (Figure 2c). For monoclinic, nonbuffered $SrRuO_3$, the rotation angles along the three orthogonal axes are extracted to be $\alpha = 6.2 \pm 1.3°$ (in-plane (+) axis), $\beta = 6.8 \pm 1.4°$ (in-plane (−) axis), and $\gamma = 7.4 \pm 1.5°$ (out-of-plane (−) axis). Two majority structural variants (D_X and $D_{X'}$) occupying ∼70% of the volume are observed. Therefore, the octahedral rotation patterns can be determined to be $a^+b^-c^-$ or $a^-b^+c^-$. For comparison, in bulk $SrRuO_3$ the rotation pattern is $a^+c^-c^-$ with $\alpha_{bulk} = 6.19°$ and $\beta_{bulk} = \gamma_{bulk} = 5.97°$.[23,31] Thus, in monoclinic, nonbuffered $SrRuO_3$, the octahedral rotation angle in the in-plane (+) axis is similar to the bulk value, but the rotations in the two (−) axes, especially the one along the [001] of $SrTiO_3$, are considerably larger and the down-selection of structural domains is consistent with prior work.[30]

Similarly, for tetragonal, buffered $SrRuO_3$, the rotation angles are extracted to be $\alpha = 5.7 \pm 1.6°$, $\beta = 5.9 \pm 1.9°$, and $\gamma = 7.2 \pm 1.4°$, which are slightly smaller than those in the monoclinic, nonbuffered variant. Surprisingly, four structural domains (D_X, D_Y, $D_{X'}$, and $D_{Y'}$) are found to occupy similar volumetric fractions in the films. Based on the preceding discussion, the octahedral rotation pattern of tetragonal $SrRuO_3$ can also be represented as $a^+b^-c^-$ or $a^-b^+c^-$. As compared to monoclinic, nonbuffered $SrRuO_3$, however, in the tetragonal variant the out-of-plane (−) axis octahedral rotation remains the same but the two in-plane rotation angles are slightly reduced. Such a decrease in the in-plane octahedral rotation angles results in an

DOI: 10.1021/acsami.6b02864
ACS Appl. Mater. Interfaces 2016, 8, 14871−14878

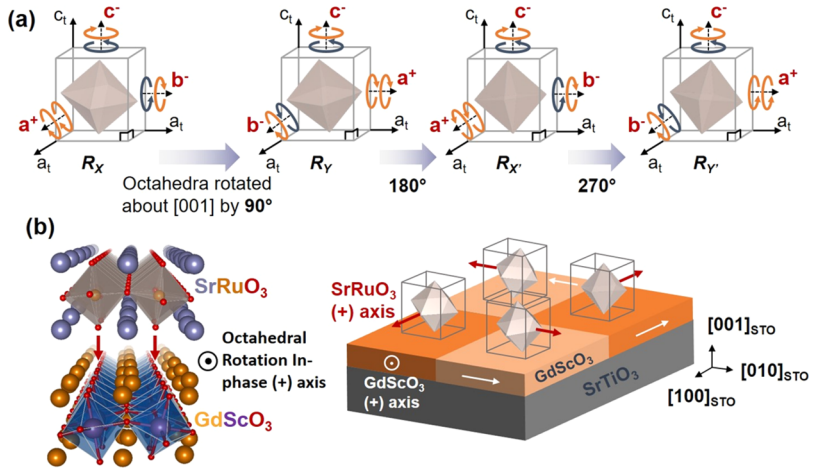

Figure 3. (a) Schematic illustration of the four octahedra "rotational" domains (R_X, R_Y, $R_{X'}$, and $R_{Y'}$) possible in the tetragonal variant of $SrRuO_3$ where the various rotational domains can be thought of as rotating the octahedra within the lattice about the [001] by 0°, 90°, 180°, or 270°. (b) Illustration of the tendency of the $SrRuO_3$ to align its in-phase (+) rotation axis with the $GdScO_3$ (+) rotation axis during growth and the corresponding coupling between $GdScO_3$ structural domains and $SrRuO_3$ rotational domains. The white arrows show the direction of the in-phase (+) octahedral rotation axis.

out-of-plane lattice expansion, while the unchanged γ angle suggests that the octahedral rotation along the out-of-plane axis is mainly controlled by lattice mismatch.

What is more surprising is the observation of four structural domains in the tetragonal variant. As the lattice possesses 4-fold symmetry about the [001], only one structural variant should be allowed. Fitting of the half-order Bragg peaks, however, suggests the presence of four different "structural" domains within the tetragonal lattice. These structural domains are the result of *different octahedral rotation patterns in the films* which, in turn, give rise to a number of half-order diffraction peaks which can be fit. From the fit, we observe four uniquely different octahedral rotation patterns where the octahedra can rotate about the [001] by 0°, 90°, 180°, or 270°, thus giving rise to what we will refer to as "rotational" domains R_X, R_Y, $R_{X'}$, and $R_{Y'}$ (Figure 3a). In other words, the combination of RSM and half-order Bragg peak analyses suggest that, in tetragonal $SrRuO_3$, it is possible to rotate the nature of the octahedral rotation independently within the lattice. The fits also reveal a nearly equivalent volume fraction of the different rotational domains (Figure 2c). We propose that this arises due to the presence of a number of rotational domains in the $GdScO_3$-buffer layer. As is common, when an orthorhombic material is grown on a cubic substrate, multiple structural variants are formed. In this case, although the results suggest that the $GdScO_3$ has an octahedral rotation pattern similar to that of $SrRuO_3$, exact fitting of this pattern is difficult because of large changes in the rotation pattern in $GdScO_3$ which is confined between nonrotated ($SrTiO_3$) and rotated ($SrRuO_3$) materials. In turn, we hypothesize that the presence of various rotational domains in the $GdScO_3$ results in uniform epitaxial growth of the tetragonal variant of $SrRuO_3$, but separation of the $SrRuO_3$ in four different rotational domains as dictated by the local octahedral rotation alignment in the $GdScO_3$-buffer layer which tends to drive the in-phase (+) rotation axis in the $GdScO_3$ and $SrRuO_3$ to be aligned (Figure 3b).

In the theory proposed by Glazer[18] that relates the octahedral rotation network and the lattice symmetry, a three-tilt system is expected to have lower lattice symmetry (e.g., triclinic or orthorhombic). For a high-symmetry lattice (e.g., tetragonal), however, it is thought that the octahedra are only allowed to rotate along one axis (i.e., $a^0a^0c^-$).[35−37] In the tetragonal, buffered $SrRuO_3$, however, we observe the presence of a three-tilting octahedral rotation pattern suggesting that the internal octahedral rotation pattern could be decoupled from the symmetry of the lattice. Similar structural changes in tensile-strained $SrRuO_3$ have been reported before, but the results suggested no/limited decoupling between oxygen octahedra and lattice symmetry.[38] Moreover, due to such a decoupling of the lattice symmetry and octahedral rotation pattern, we are able to observe multiple rotational domains in a tetragonal lattice. It is important to note that such decoupling is fundamentally allowed because, within the calculation framework of Glazer, the displacement of cations is not considered, and thus the symmetry given by the octahedral network and the symmetry given by cations could potentially be considered separately. Such decoupling is likely to be a generic feature of perovskite oxide thin films, but the magnitude of this effect could vary depending on the extent of hybridization of the states arising from the *A*-site cation and those of the *B*-site and anion lattice. For instance, similar results have been reported for $SrTiO_3$ thin films grown on tensile substrates wherein the lattice appears to be tetragonal while the internal octahedral rotation pattern belongs to orthorhombic symmetry group *Cmcm*.[39] Likewise, for $BiFeO_3$ films on $(LaAlO_3)_{0.3}$-$(Sr_2AlTaO_6)_{0.7}$ substrates, the tetragonal lattice as probed by synchrotron radiation contains a monoclinic, polar symmetry.[40] Such findings deserve further studies and could be potentially useful in designing novel ultrathin/superlattice perovskite systems. Note that we additionally considered other potential explanations for the observed data which were subsequently ruled out or considered to be unlikely (see Supporting Information, Figures S6 and S7).

Armed with this detailed understanding of the lattice symmetry and octahedral rotations, we proceeded to explore how such effects could drive changes in the physical properties of $SrRuO_3$. Temperature-dependent resistivity measurements from 25 to 250 K in the van der Pauw geometry[41] (Figure 4) reveal the high quality of the $SrRuO_3$ heterostructures as indicated by the overall low resistivity (10^{-5}−10^{-4} Ω·cm) and the relatively large ratio (4−6) between high- and low-

DOI: 10.1021/acsami.6b02864
ACS Appl. Mater. Interfaces 2016, 8, 14871−14878

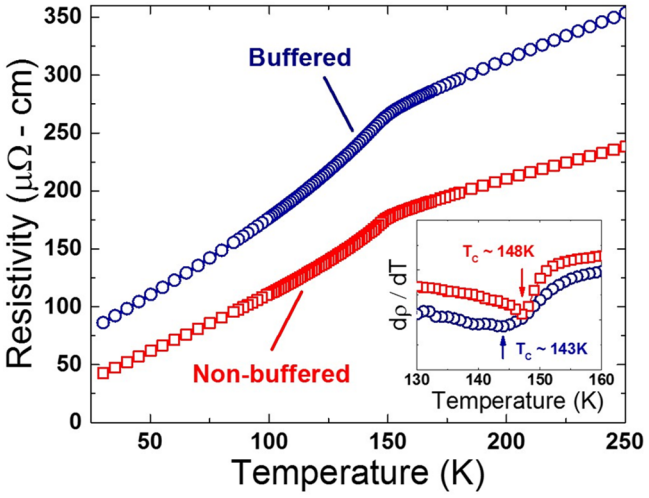

Figure 4. Temperature-dependent electrical resistivity behavior for 10 nm thick nonbuffered (red squares) and buffered (blue circles) $SrRuO_3$ heterostructures. The inset shows $\frac{d\rho}{dT}$ vs T curves and demarcates the T_C.

temperature resistivities ($\frac{\rho_{250K}}{\rho_{25K}}$).[9] In general, it has been argued that epitaxial strain,[12] film thickness,[35,42] and stoichiometry[43] can significantly affect the film structure (i.e., Ru−O−Ru bond angle) thereby giving rise to changes in hybridization between the Ru 4*d* orbitals and the O 2*p* orbitals which will manifest in marked changes in the macroscopic electrical transport. From this work, however, in a situation where we have controlled film thickness, stoichiometry, crystallinity, and strain state to be the same, the mere insertion of the $GdScO_3$-buffer layer (and the subsequent changes in the lattice symmetry and in-plane octahedral rotation angles of $SrRuO_3$) results in an decrease in T_C by ∼5 K and gives rise to a large increase in the overall film resistivity (over 100% at low temperature).

We additionally studied the magnetic properties of buffered and nonbuffered $SrRuO_3$ heterostructures. Hysteresis loops for the monoclinic, nonbuffered $SrRuO_3$ (Figure 5a) reveal that the $SrRuO_3$ films have an out-of-plane easy axis that gives a saturated magnetization of ∼1.46 μ_B/Ru (∼225 emu/cm^3) and projects anisotropically onto [100] and [010]. Additionally, a sharp magnetic phase transition was observed in the temperature dependence of the nonbuffered $SrRuO_3$, and the T_C was determined to be ∼148 K (Figure 5b). Upon insertion of the $GdScO_3$-buffer layer and transformation of the $SrRuO_3$ film to tetragonal symmetry, the films still exhibit an out-of-plane easy axis, but with nearly isotropic in-plane magnetic response (Figure 5c). Such isotropic magnetic behavior could be attributed to the symmetry change of the unit cell such that the easy axis is more aligned with the out-of-plane axis. Additionally, we note that the presence of multiple rotational domain variants in these samples could also give rise to an effectively averaged magnetic response in the buffered $SrRuO_3$ which could also contribute to the more isotropic in-plane magnetization. Additionally, the out-of-plane magnetization was also found to be decreased to ∼1.06 μ_B/Ru (∼165 emu/cm^3). In $SrRuO_3$, the magnetization is strongly coupled with the orthorhombicity of the unit cell, and as has been calculated,[44] increasing the unit cell symmetry from orthorhombic to cubic will lower the ground-state magnetic moments. Thus, the smaller saturated magnetic moments that we observed in the $SrRuO_3$ films grown on buffered $SrTiO_3$ are consistent with an increase in the symmetry of the film. Likewise, in the tetragonal variant of $SrRuO_3$, a reduction of T_C to ∼143 K was observed

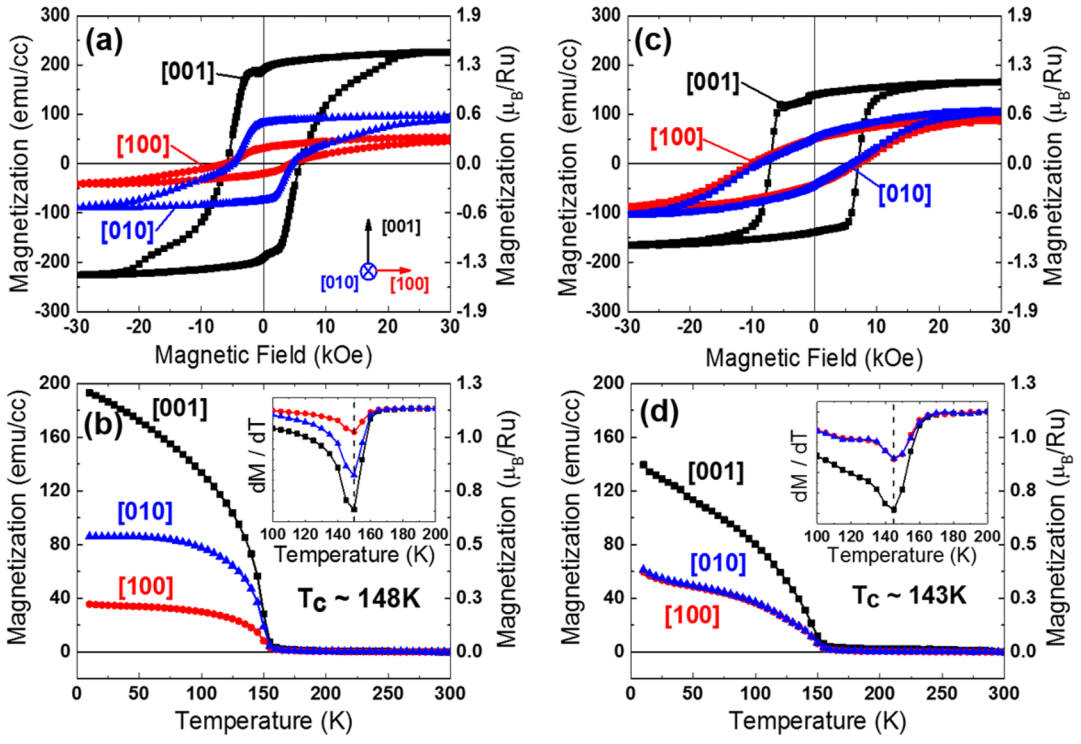

Figure 5. Magnetization−magnetic field and magnetization−temperature results for 10 nm thick (a, b) nonbuffered and (c, d) buffered $SrRuO_3$ heterostructures. All samples are cooled at 1 T field from room temperature to 10 K prior to study.

DOI: 10.1021/acsami.6b02864
ACS Appl. Mater. Interfaces 2016, 8, 14871−14878

(Figure 5d), consistent with the observations from the electronic transport.

CONCLUSION

In summary, we have demonstrated that for buffered and nonbuffered $SrRuO_3$ films, even under the same lattice mismatch strain, one is able to change the film lattice symmetry and corresponding electrical and magnetic behavior by changing the interfacial octahedral rotation patterns. Detailed structural studies via half-order Bragg peak analysis have revealed that the octahedral rotation pattern of buffered and nonbuffered $SrRuO_3$ are both $a^+b^-c^-$, while the in-plane octahedral rotation angles are reduced in those grown on nonbuffered substrates and nearly equal fractions of "rotational" domain are observed. The observed $a^+b^-c^-$ octahedral rotation pattern in tetragonal variants of $SrRuO_3$ suggests that the symmetry of the octahedral rotation network as described by Glazer can actually be decoupled from the symmetry of the overall lattice. These results, in turn, provide new insights into novel ways of engineering structure and physical properties of perovskite thin films and lead to better understanding of the interaction between strain, octahedral behavior, and crystal symmetry in perovskite oxide thin films.

ASSOCIATED CONTENT

Supporting Information

The Supporting Information is available free of charge on the ACS Publications website at DOI: 10.1021/acsami.6b02864.

Additional X-ray diffraction studies and structural variants, $GdScO_3$-buffer-layer structure, additional evidence for tetragonal lattice symmetry in buffered $SrRuO_3$ films, and $SrRuO_3$ octahedral rotation angles and domain structure determination (PDF)

AUTHOR INFORMATION

Corresponding Authors

*(L.W.M.) E-mail: lwmartin@berkeley.edu.
*(Z.C.) E-mail: zuhuang@berkeley.edu.

Notes

The authors declare no competing financial interest.

ACKNOWLEDGMENTS

R. Gao acknowledges support from the Air Force Office of Scientific Research under Grant FA9550-12-1-0471. Y.Q.D., H.X., Z.L.L., and C. Gao acknowledge the support from 12-ID-D at the Advanced Photon Source and 14B at Shanghai Synchrotron Radiation Facility. Z.L.L. also acknowledges the support from the National Natural Science Foundation of China (Grant Nos. 11374010 and 11434009). H.Z. acknowledges support from the resources of the Advanced Photon Source, a U.S. Department of Energy (DOE) Office of Science User Facility operated for the DOE Office of Science by Argonne National Laboratory under Contract No. DE-AC02-06CH11357. Y.Y. and V.G. gratefully acknowledge support from the Penn State MRSEC Center for Nanoscale Science, Grant DMR-1420620. D.D.F. acknowledges support from the U.S. Department of Energy Office of Science, Basic Energy Sciences, Materials Sciences and Engineering Division. Z.C. acknowledges support from the Laboratory Directed Research and Development Program of Lawrence Berkeley National Laboratory under U.S. Department of Energy Contract No. DE-AC02-05CH11231 for the development of the $SrRuO_3$ films. L.W.M. acknowledges support from the U.S. Department of Energy, Office of Basic Energy Science under Contract No. DE-SC0012375 for the development of metastable $SrRuO_3$ structures.

REFERENCES

(1) Imada, M.; Fujimori, A.; Tokura, Y. Metal-Insulator Transitions. *Rev. Mod. Phys.* **1998**, *70*, 1039−1263.
(2) Mannhart, J.; Schlom, D. G. Oxide Interfaces—An Opportunity for Electronics. *Science* **2010**, *327*, 1607−1611.
(3) Scott, J. F. Applications of Modern Ferroelectrics. *Science* **2007**, *315*, 954−959.
(4) Tadigadapa, S.; Mateti, K. Piezoelectric MEMS Sensors: State-of-the-Art and Perspectives. *Meas. Sci. Technol.* **2009**, *20*, 092001.
(5) Grinberg, I.; West, D. V.; Torres, M.; Gou, G.; Stein, D. M.; Wu, L.; Chen, G.; Gallo, E. M.; Akbashev, A. R.; Davies, P. K.; Spanier, J. E.; Rappe, A. M. Perovskite Oxides for Visible-Light-Absorbing Ferroelectric and Photovoltaic Materials. *Nature* **2013**, *503*, 509−512.
(6) Hwang, H. Y.; Iwasa, Y.; Kawasaki, M.; Keimer, B.; Nagaosa, N.; Tokura, Y. Emergent Phenomena at Oxide Interfaces. *Nat. Mater.* **2012**, *11*, 103−113.
(7) Rondinelli, J. M.; Spaldin, N. A. Structure and Properties of Functional Oxide Thin Films: Insights from Electronic-Structure Calculations. *Adv. Mater.* **2011**, *23*, 3363−3381.
(8) Zubko, P.; Gariglio, S.; Gabay, M.; Ghosez, P.; Triscone, J.-M. Interface Physics in Complex Oxide Heterostructures. *Annu. Rev. Condens. Matter Phys.* **2011**, *2*, 141−165.
(9) Koster, G.; Klein, L.; Siemons, W.; Rijnders, G.; Dodge, J. S.; Eom, C.-B.; Blank, D. H. A.; Beasley, M. R. Structure, Physical Properties, and Applications of $SrRuO_3$ Thin Films. *Rev. Mod. Phys.* **2012**, *84*, 253−298.
(10) Gan, Q.; Rao, R. A.; Eom, C. B.; Garrett, J. L.; Lee, M. Direct Measurement of Strain Effects on Magnetic and Electrical Properties of Epitaxial $SrRuO_3$ Thin Films. *Appl. Phys. Lett.* **1998**, *72*, 978−980.
(11) Grutter, A. J.; Wong, F. J.; Jenkins, C. A.; Arenholz, E.; Vailionis, A.; Suzuki, Y. Stabilization of Spin-Zero Ru^{4+} Through Epitaxial Strain in $SrRuO_3$ Thin Films. *Phys. Rev. B: Condens. Matter Mater. Phys.* **2013**, *88*, 214410.
(12) Zayak, A. T.; Huang, X.; Neaton, J. B.; Rabe, K. M. Structural, Electronic, and Magnetic Properties of $SrRuO_3$ under Epitaxial Strain. *Phys. Rev. B: Condens. Matter Mater. Phys.* **2006**, *74*, 094104.
(13) Kan, D.; Aso, R.; Kurata, H.; Shimakawa, Y. Epitaxial Strain Effect in Tetragonal $SrRuO_3$ Thin Films. *J. Appl. Phys.* **2013**, *113*, 173912.
(14) Vailionis, A.; Siemons, W.; Koster, G. Room Temperature Epitaxial Stabilization of a Tetragonal Phase in $ARuO_3$ (A = Ca and Sr) Thin Films. *Appl. Phys. Lett.* **2008**, *93*, 051909.
(15) He, J.; Borisevich, A.; Kalinin, S. V.; Pennycook, S. J.; Pantelides, S. T. Control of Octahedral Tilts and Magnetic Properties of Perovskite Oxide Heterostructures by Substrate Symmetry. *Phys. Rev. Lett.* **2010**, *105*, 227203.
(16) Rondinelli, J. M.; May, S. J.; Freeland, J. W. Control of Octahedral Connectivity in Perovskite Oxide Heterostructures: An Emerging Route to Multifunctional Materials Discovery. *MRS Bull.* **2012**, *37*, 261−270.
(17) Rondinelli, J. M.; Spaldin, N. A. Substrate Coherency Driven Octahedral Rotations in Perovskite Oxide Films. *Phys. Rev. B: Condens. Matter Mater. Phys.* **2010**, *82*, 113402.
(18) Glazer, A. M. The Classification of Tilted Octahedra in Perovskites. *Acta Crystallogr., Sect. B: Struct. Crystallogr. Cryst. Chem.* **1972**, *28*, 3384−3392.
(19) Woodward, P. M. Octahedral Tilting in Perovskites. I. Geometrical Considerations. *Acta Crystallogr., Sect. B: Struct. Sci.* **1997**, *53*, 32−43.
(20) Woodward, P. M. Octahedral Tilting in Perovskites. II. Structure Stabilizing Forces. *Acta Crystallogr., Sect. B: Struct. Sci.* **1997**, *53*, 44−66.

DOI: 10.1021/acsami.6b02864
ACS Appl. Mater. Interfaces 2016, 8, 14871−14878

(21) Borisevich, A. Y.; Chang, H. J.; Huijben, M.; Oxley, M. P.; Okamoto, S.; Niranjan, M. K.; Burton, J. D.; Tsymbal, E. Y.; Chu, Y. H.; Yu, P.; Ramesh, R.; Kalinin, S. V.; Pennycook, S. J. Suppression of Octahedral Tilts and Associated Changes in Electronic Properties at Epitaxial Oxide Heterostructure Interfaces. *Phys. Rev. Lett.* **2010**, *105*, 087204.
(22) Jia, C. L.; Mi, S. B.; Faley, M.; Poppe, U.; Schubert, J.; Urban, K. Oxygen Octahedron Reconstruction in the $SrTiO_3/LaAlO_3$ Heterointerfaces Investigated Using Aberration-Corrected Ultrahigh-Resolution Transmission Electron Microscopy. *Phys. Rev. B: Condens. Matter Mater. Phys.* **2009**, *79*, 081405.
(23) May, S. J.; Smith, C. R.; Kim, J. W.; Karapetrova, E.; Bhattacharya, A.; Ryan, P. J. Control of Octahedral Rotations in $(LaNiO_3)_n/(SrMnO_3)_m$ Superlattices. *Phys. Rev. B: Condens. Matter Mater. Phys.* **2011**, *83*, 153411.
(24) Chakoumakos, B. C.; Schlom, D. G.; Urbanik, M.; Luine, J. Thermal Expansion of $LaAlO_3$ and (La,Sr) (Al,Ta)O_3, Substrate Materials for Superconducting Thin-Film Device Applications. *J. Appl. Phys.* **1998**, *83*, 1979−1982.
(25) Lytle, F. W. X-Ray Diffractometry of Low-Temperature Phase Transformations in Strontium Titanate. *J. Appl. Phys.* **1964**, *35*, 2212−2215.
(26) Vasylechko, L.; Matkovskii, A.; Savytskii, D.; Suchocki, A.; Wallrafen, F. Crystal Structure of $GdFeO_3$-Type Rare Earth Gallates and Aluminates. *J. Alloys Compd.* **1999**, *291*, 57−65.
(27) Veličkov, B.; Kahlenberg, V.; Bertram, R.; Bernhagen, M. Crystal Chemistry of $GdScO_3$, $DyScO_3$, $SmScO_3$ and $NdScO_3$. *Z. Kristallogr.* **2007**, *222*, 466−473.
(28) Chen, Z. H.; Damodaran, A. R.; Xu, R.; Lee, S.; Martin, L. W. Effect of "Symmetry Mismatch" on the Domain Structure of Rhombohedral $BiFeO_3$ Thin Films. *Appl. Phys. Lett.* **2014**, *104*, 182908.
(29) Kawasaki, M.; Takahashi, K.; Maeda, T.; Tsuchiya, R.; Shinohara, M.; Ishiyama, O.; Yonezawa, T.; Yoshimoto, M.; Koinuma, H. Atomic Control of the $SrTiO_3$ Crystal Surface. *Science* **1994**, *266*, 1540−1542.
(30) Jiang, J. C.; Tian, W.; Pan, X. Q.; Gan, Q.; Eom, C. B. Domain Structure of Epitaxial $SrRuO_3$ Thin Films on Miscut (001) $SrTiO_3$ Substrates. *Appl. Phys. Lett.* **1998**, *72*, 2963−2965.
(31) Jones, C. W.; Battle, P. D.; Lightfoot, P.; Harrison, W. T. A. The Structure of $SrRuO_3$ by Time-of-Flight Neutron Powder Diffraction. *Acta Crystallogr., Sect. C: Cryst. Struct. Commun.* **1989**, *45*, 365−367.
(32) Aso, R.; Kan, D.; Shimakawa, Y.; Kurata, H. Atomic Level Observation of Octahedral Distortions at the Perovskite Oxide Heterointerface. *Sci. Rep.* **2013**, *3*, 2214−2219.
(33) Glazer, A. M. Simple Ways of Determining Perovskite Structures. *Acta Crystallogr., Sect. A: Cryst. Phys., Diffr., Theor. Gen. Crystallogr.* **1975**, *31*, 756−762.
(34) May, S. J.; Kim, J. W.; Rondinelli, J. M.; Karapetrova, E.; Spaldin, N. A.; Bhattacharya, A.; Ryan, P. J. Quantifying Octahedral Rotations in Strained Perovskite Oxide Films. *Phys. Rev. B: Condens. Matter Mater. Phys.* **2010**, *82*, 014110.
(35) Chang, S. H.; Chang, Y. J.; Jang, S. Y.; Jeong, D. W.; Jung, C. U.; Kim, Y. J.; Chung, J. S.; Noh, T. W. Thickness-Dependent Structural Phase Transition of Strained $SrRuO_3$ Ultrathin Films: The Role of Octahedral Tilt. *Phys. Rev. B: Condens. Matter Mater. Phys.* **2011**, *84*, 104101.
(36) Lu, W.; Yang, P.; Song, W. D.; Chow, G. M.; Chen, J. S. Control of Oxygen Octahedral Rotations and Physical Properties in $SrRuO_3$ Films. *Phys. Rev. B: Condens. Matter Mater. Phys.* **2013**, *88*, 214115.
(37) Vailionis, A.; Boschker, H.; Siemons, W.; Houwman, E. P.; Blank, D. H. A.; Rijnders, G.; Koster, G. Misfit Strain Accommodation in Epitaxial ABO_3 Perovskites: Lattice Rotations and Lattice Modulations. *Phys. Rev. B: Condens. Matter Mater. Phys.* **2011**, *83*, 064101.
(38) Aso, R.; Kan, D.; Shimakawa, Y.; Kurata, H. Control of Structural Distortions in Transition-Metal Oxide Films through Oxygen Displacement at the Heterointerface. *Adv. Funct. Mater.* **2014**, *24*, 5177−5184.
(39) He, F.; Wells, B. O.; Shapiro, S. M. Strain Phase Diagram and Domain Orientation in $SrTiO_3$ Thin Films. *Phys. Rev. Lett.* **2005**, *94*, 176101.
(40) Chen, Z.; Zou, X.; Ren, W.; You, L.; Huang, C.; Yang, Y.; Yang, P.; Wang, J.; Sritharan, T.; Bellaiche, L.; Chen, L. Study of Strain Effect on In-plane Polarization in Epitaxial $BiFeO_3$ Thin Films Using Planar Electrodes. *Phys. Rev. B: Condens. Matter Mater. Phys.* **2012**, *86*, 235125.
(41) van der Pauw, L. J. A Method of Measuring Specific Resistivity and Hall Effect of Discs of Arbitrary Shape. *Philips Res. Rep.* **1958**, *13*, 1−9.
(42) Chang, Y. J.; Kim, C. H.; Phark, S. H.; Kim, Y. S.; Yu, J.; Noh, T. W. Fundamental Thickness Limit of Itinerant Ferromagnetic $SrRuO_3$ Thin Films. *Phys. Rev. Lett.* **2009**, *103*, 057201.
(43) Siemons, W.; Koster, G.; Vailionis, A.; Yamamoto, H.; Blank, D. H. A.; Beasley, M. R. Dependence of the Electronic Structure of $SrRuO_3$ and Its Degree of Correlation on Cation Off-Stoichiometry. *Phys. Rev. B: Condens. Matter Mater. Phys.* **2007**, *76*, 075126.
(44) Singh, D. J. Electronic and Magnetic Properties of the 4d Itinerant Ferromagnet $SrRuO_3$. *J. Appl. Phys.* **1996**, *79*, 4818−4820.

DOI: 10.1021/acsami.6b02864
ACS Appl. Mater. Interfaces 2016, 8, 14871−14878